# Divergent trends of ecosystem-scale photosynthetic efficiency between arid and humid lands across the globe

**Running title:** Ecosystem-scale photosynthetic efficiency

Fangli Wei, Shuai Wang, Bojie Fu, Lanhui Wang, Wenmin Zhang, Lixin Wang, Ning Pan, Rasmus Fensholt

**Abstract**

**Aim:** A widespread greening and an increasing global terrestrial carbon sink over recent decades have been reported. However, the spatio-temporal relationships between vegetation greenness and productivity and the factors influencing this relationship remain unclear. We define a new metric of ecosystem-scale photosynthetic efficiency (EPE) to analyze its spatio-temporal pattern and investigate how potential drivers regulate the greenness-productivity relationship.

**Location:** Global

**Time period:** From 2001 to 2016

**Major taxa studied:** Global terrestrial ecosystems

**Methods:** This study used global datasets of leaf area index (LAI) and solar-induced fluorescence (SIF) as proxies of vegetation greenness and ecosystem productivity, respectively, to propose a new metric of SIF/LAI representing ecosystem-scale photosynthetic efficiency (EPE). We identified the spatial pattern and dynamics of EPE and examined factors influencing EPE.

**Results:** The results showed a weaker increase in productivity compared to the global greening rate from 2001 to 2016, suggesting a decline in EPE at the global scale. This decline in EPE indicates a disproportionate increase in terrestrial productivity against the widespread greening. When stratified into areas following an aridity gradient, we found that EPE overall showed upward trends in arid and semi-arid areas, and downward trends in dry sub-humid and humid regions. The EPE was primarily controlled by soil moisture that promoted and constrained the EPE in xeric and mesic ecosystems, respectively. Meanwhile, the increased short vegetation cover and

---

This is the author's manuscript of the article published in final edited form as:

Wei, F., Wang, S., Fu, B., Wang, L., Zhang, W., Wang, L., Pan, N., & Fensholt, R. (2022). Divergent trends of ecosystem-scale photosynthetic efficiency between arid and humid lands across the globe. Global Ecology and Biogeography, 31(9), 1824–1837. https://doi.org/10.1111/geb.13561

atmospheric water demand positively and negatively contributed to EPE changes in xeric and mesic ecosystems.

**Main conclusions:** Our study shows that Earth greening is associated with decreasing EPE, revealing that current rates of carbon sequestration does not increase proportionally to Earth's greening, and highlights soil moisture is a key controller of EPE. These results help reduce the uncertainties of future climate change impacts on vegetation dynamics, thus having implications for sustainable ecosystem management and climate change mitigation.

**Keywords:** photosynthetic efficiency; leaf area index; solar-induced fluorescence; aridity gradients; soil moisture; atmospheric water vapor pressure

# 1. Introduction

As the critical component of the biosphere, terrestrial vegetation regulates the exchange of carbon, water, and energy between the land and the atmosphere and provides vital ecosystem services for human beings (Pettorelli et al., 2005; Piao et al., 2019). Changes in ecosystem structure (e.g., greenness, composition) and function (e.g., ecosystem productivity, biomass) are driven by climatic changes and human activities (Chen et al., 2019a; Chen et al., 2019b; Piao et al., 2019). A plethora of studies based on state-of-the-art earth observation datasets have shown a widespread greening and an increase in ecosystem productivity over the past decades (Huang et al., 2018; Zhu et al., 2016), also supported by evidence from ground-based vegetation inventories and global ecosystem models (Chen et al., 2019b; Piao et al., 2019). However, it is currently unknown if the greening has led to a proportional increase in primary production, as the photosynthetic functioning of green leaves is also determined by environmental conditions and might be sensitive to climatic extremes (Poulter et al., 2014; Yang et al., 2018).

Recently, several studies have challenged the long-held narrative of the positive relationship between vegetation greenness and productivity and reported inconsistent changes between these two, particularly at short time scales (Smith et al., 2018; Yan et

al., 2019; Yang et al., 2018). For example, satellite chlorophyll fluorescence measurements reveal large-scale decoupling of photosynthesis and greenness dynamics in boreal evergreen forests (Walther et al., 2016). Using vegetation greenness as a proxy for productivity is not always valid. For example, EVI cannot capture the seasonal and interannual GPP dynamics well in dryland ecosystems of southwestern North America (Smith et al., 2018). Moreover, photosynthesis is more sensitive to environmental change than is the case for vegetation greenness (Yan et al., 2019). Thus, environmental factors could lead to a notable change in ecosystem productivity before being observable through changes in vegetation greenness (Smith et al., 2018). Therefore, large uncertainties remain in current knowledge of the spatiotemporal relationships between vegetation greenness and productivity on a global scale, and also a gap in our understanding exists of what factors influence and how they regulate this relationship.

Remote sensing is poised to reveal the global pattern of vegetation greenness-productivity relationship and its dynamics. Solar-induced chlorophyll fluorescence (SIF) has shown great potential to monitor the photosynthetic activity of terrestrial ecosystems (Frankenberg et al., 2011; Joiner et al., 2011), which is mechanistically linked to gross primary productivity (GPP) through light use efficiency and the fraction of absorbed photosynthetically active radiation (fAPAR) quenched in the photochemical and fluorescence pathway (Damm et al., 2015; Ryu et al., 2019). When measured by satellite, SIF has shown a near-linear relationship with GPP at the ecosystem scale (Sun et al., 2018; Xiao et al., 2019). The leaf area index (LAI) measures the active photosynthetic area and the area subjected to transpiration, which is a good indicator of vegetation greenness or foliage biomass (Kaufmann et al., 1981; Piao et al., 2019). Consequently, we use SIF as a proxy for GPP and LAI as an indicator of greenness to investigate the relationship between vegetation greenness and productivity.

Here we defined a new metric as the ratio of ecosystem productivity to greenness (SIF/LAI), which quantifies the capacity of photosynthesis per unit leaf area and thus can be used as an indicator of ecosystem-scale photosynthetic efficiency (EPE). The

significant trends of EPE (i.e., SIF/LAI) indicate the different/disproportionate changes between vegetation greenness and productivity. If the trend of EPE is positive, this means that SIF increases more than LAI increases or SIF decreases less than LAI decreases, and vice versa for a negative trend of EPE. Based on the above definition of EPE and the explanations of its trends, we aimed to identify the spatiotemporal pattern of EPE and analyze the potential drivers affecting it. The three main research steps involve the following: (1) identifying the global pattern of EPE and its trends during 2001-2016; (2) analyzing how EPE and its trends vary along an aridity gradient and with land cover types (Fig. 1); (3) investigating what factors influence EPE and in which way. The newly proposed EPE concept is an essential first step towards the mechanistic understanding of the pattern of Earth greening and the role of the terrestrial biosphere in the global carbon cycle, thus helping build knowledge of sustainable ecosystem management and climate change mitigation.

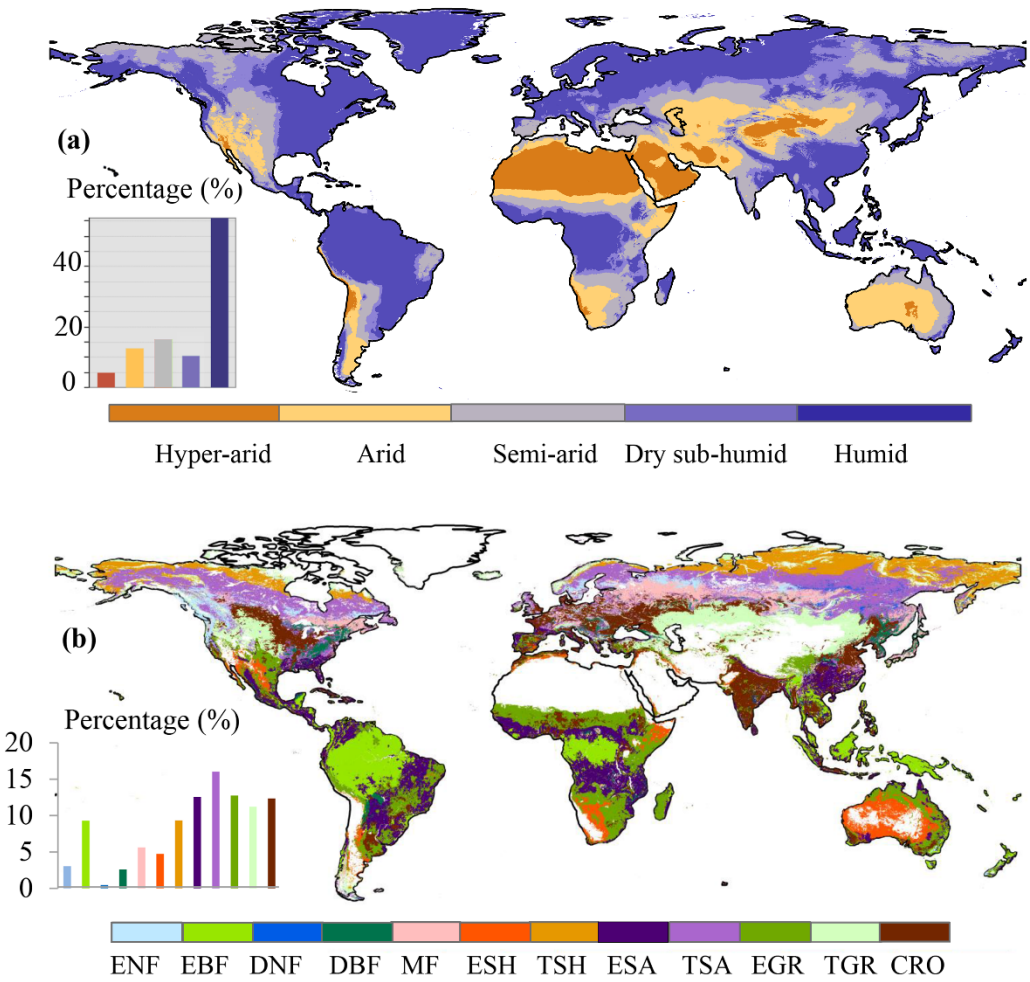

**Fig. 1.** Global distribution of aridity classes and land-cover types. (a) Aridity classes, (b) land cover types. Aridity classes are based on Global Aridity Index datasets. Here the hyper-arid area was excluded from our analysis. Land cover types were produced by combing the Global thermal climate zone map and MCD12 land cover product (MCD12Q1). ENF: evergreen needleleaf forest; EBF: evergreen broadleaf forest; DNF: deciduous needleleaf forest; DBF: deciduous broadleaf forest; MF: mixed forest; TSH: tropical shrublands; ESH: extratropical shrublands; TSA: tropical savannas; ESA: extratropical savannas; TGR: tropical grasslands; EGR: extratropical grasslands; CRO: croplands. Here only stable pixels where no changes in the dominant land cover class during 2001–2016 were displayed.

# 2. Materials and methods

## 2.1 Datasets

**Aridity classes.** The aridity index is defined as the ratio of total annual precipitation to potential evapotranspiration (PET) and can be used to measure the aridity of a region. According to this indicator, global lands are stratified into five classes: hyper-arid (AI < 0.05), arid (0.05 ≤ AI < 0.2), semi-arid (0.2 ≤ AI < 0.5), dry sub-humid (0.5 ≤ AI < 0.65), and humid regions (AI ≥ 0.65, Middleton, 1997). We adopted the average aridity index based on precipitation and evapotranspiration datasets from WorldClim 2.0 (Antonio and Robert, 2019).

**Land cover types.** By combing the Global thermal climate zone map (derived from http://www.fao.org/geonetwork/srv/en/metadata.show?id=14056&currTab=simple) with MCD12 land cover product (MCD12Q1) (Sulla-Menashe and Friedl, 2018), we classified the global lands into 12 land cover types, including evergreen needleleaf forest (ENF); evergreen broadleaf forest (EBF); deciduous needleleaf forest (DNF); deciduous broadleaf forest (DBF); mixed forest (MF); tropical shrublands (TSH); extratropical shrublands (ESH); tropical savannas (TSA); extratropical savannas (ESA); tropical grasslands (TGA); extratropical grasslands (EGA); croplands (CRO). To reduce the impacts of classification error and land cover change, only stable pixels—defined as areas with no change in the dominant land cover class during 2001 – 2016—were used to define the above-mentioned 12 land cover types (Forzieri et al., 2017). The spatial resolution of land cover is 500 meter, which was resampled to a 0.05° spatial resolution using nearest neighbour interpolation.

**Solar-induced chlorophyll fluorescence (SIF).** In this study, we used a globally continuous coverage and high spatial resolution (0.05° × 0.05°) SIF (GOSIF) dataset over the period 2001-2016 (Li and Xiao, 2019), which was produced by training a neural network (NN) with surface reflectance from the Moderate Resolution Imaging Spectroradiometer (MODIS) and SIF from Orbiting Carbon Observatory-2 (OCO-2). SIF is an optical signal that is emitted from vegetation when sunlight activates photosynthesis. Our study uses SIF as a proxy for GPP because SIF is mechanistically linked to GPP and has shown a near-linear relationship with GPP at the ecosystem scale when measured by satellite (Xiao et al., 2019). Moreover, we also used another global spatially contiguous SIF (CSIF) dataset at a high spatial resolution (0.05° × 0.05°) during 2001-2016 to check whether the changes in SIF are robust (Zhang et al., 2018).

**Gross primary production (GPP).** The global GPP dataset over the period 2001-2016 derived from the vegetation photosynthesis model (VPM), with a 0.05° spatial resolution, based on an improved light use efficiency theory which uses the energy absorbed by chlorophyll and driven by satellite data from MODIS and climate data from NCEP Reanalysis II (Zhang et al., 2017). The VPM algorithm uses the energy absorbed by chlorophyll, thus can better capture the seasonal and inter-annual variations of vegetation photosynthetic capacity and greatly improve the seasonal representation of GPP. $GPP_{VPM}$ showed superior performance regarding site-level validations across a wide range of land cover types (Wang et al., 2016).

**Leaf area index (LAI).** GLOBMAP_v3 LAI at a 0.08° resolution for 2001-2016 was derived from the MOD09AI C6 land surface reflectance and the associated illumination and view angles based on the GLOBCARBON LAI algorithm, which was developed based on the 4-Scale geometric optical model (Deng et al., 2006). This algorithm explicitly considers the effects of the bidirectional reflectance distribution function on reflectance over the canopy as measured by the sensors. We resampled the LAI to a 0.05° spatial resolution using nearest neighbour interpolation. Moreover, we also used SPOT LAI at a resolution of 1km during 2001-2016 to check whether the

changes in LAI are robust.

**Vegetation continuous fields (VCF).** The MODIS VCF data (MOD44B) is a yearly product that contains information about surface vegetation cover as gradations of three ground cover components: percent tree cover, percent short vegetation cover, and percent non-vegetated (DiMiceli et al., 2015), which has been widely used to detect land change and deforestation. The VCF percent tree cover layer defines a tree as any woody plant greater than or equal to 5 meters in height. Tree/short vegetation cover is the percentage of shy light in a plane orthogonal to the ground intercepted by plants defined as trees/short vegetation. The VCF data with a 250 meter pixel resolution from 2001 to 2016 was resampled to a 0.05° spatial resolution using nearest neighbour interpolation.

**Hydrometeorological variables**. This study considered plant water stress from two aspects of soil moisture supply and atmospheric water demand. Soil moisture (mm $mm^{-1}$) data was obtained from the Global Land Evaporation Amsterdam Model (GLEAM) dataset (Detsch et al., 2016). Water vapor pressure deficit (VPD) refers to the atmospheric water demand for plants, which can be calculated by the difference between the saturated water vapor pressure, determined by near-surface temperature, and the actual water vapor pressure, determined by saturated water vapor pressure and relative humidity. Relative humidity was obtained from ERA-Interim (Berrisford et al., 2011). Please see more details of VPD calculation (Yuan et al., 2019). Photosynthetically active radiation (PAR) was obtained from the NASA Langley Research Center, Cloud and Earth's Radiant Energy System (CERES, (Wielicki et al., 1996). Total PAR was calculated as the sum of surface diffusive and direct PAR in the all-sky conditions. The near-surface minimum air temperature was acquired from the latest Climate Research Unit (CRU; TS v.4.03) datasets provided by the University of East Anglia (Jones, 2018). All hydrometeorological variables data were derived from 2001 to 2016 and resampled to a 0.05° spatial resolution using nearest neighbour interpolation.

## 2.2 Analysis

**Trend analysis.** We used a non-parametric trend test technique (Mann-Kendall test), which does not require a specific sample distribution and is free from interference by outliers (Hamed and Rao, 1998), to evaluate trends in annual average SIF, LAI, SIF/LAI, tree cover, short vegetation cover, and hydrometeorological variables (i.e., minimum temperature, radiation soil moisture, VPD) at the pixel level during the period of 2001-2016. The Mann-Kendall trend test was performed using the function 'zyp.trend.vector' with the Yue–Pilon prewhitening method provided by R package 'zyp' (Bronaugh and Werner, 2013). The trends with $p \leq 0.05$ are considered to be statistically significant in this study.

**The calculation of EPE.** In this study, we defined EPE as the ratio of ecosystem productivity to greenness (SIF/LAI), which quantifies the capacity of photosynthesis per unit leaf area. Here, the main results on the spatio-temporal pattern of EPE and the driving mechanisms were based on GLOBMAP LAI and GOSIF datasets. To give uncertainty information on EPE, we also used different combinations of datasets (GOSIF and GLOBMAP LAI, CSIF and GLOBMAP LAI, GOSIF and SPOT LAI, and CSIF and SPOT LAI) to analyze the spatio-temporal patterns of EPE.

**The relative importance of potential driving variables.** Here, we used the Principle Component Analysis (PCA) and Regression (PCR) to identify the dominant driver and quantify the relative importance of variables potentially driving EPE (i.e., SIF/LAI) changes in each pixel, which eliminate the collinearity between the explainable variables (Abel et al., 2020). On a per-pixel level, through the PCA, we transform the input variables, which have been normalized by the standard deviation, into a set of new variables, the principal components (PC), which are now uncorrelated but still explain all the variation in the data. Each of the components has scores and loadings, with the latter indicating the correlations between principal components and the input variables. We then performed a multiple linear regression with the SIF/LAI as the dependent variable and the PCs as independent variables, multiplied the regression slope from the PCR with the respective loadings from the

PCA and summed the absolute values of these scores. Thus, we obtained a per-pixel estimate of the relative importance of each potential driving variable on the SIF/LAI. The factor with the largest relative importance was identified as the dominant factor.

# 3. Results

## 3.1 The spatial pattern and dynamics of EPE

The global pattern of annual mean EPE (the ratio of productivity and greenness as SIF/LAI) is spatially varying (Fig. 2a). The largest EPE appeared in the Sahel, southern Africa, Somalia, northern Australia, eastern Brazil, southern America, and India. These regions mainly comprise shrublands, savannas, and grasslands. In contrast, tropical and boreal forests have relatively low values of EPE (Fig. 2a). Although the spatial pattern of LAI trends matched to some extent with that of SIF trends (Fig. S1), changes in EPE are nonuniform (Fig. 2b). We found 22.2 % of global vegetated areas experienced significant ($p<0.05$) changes in EPE during 2001-2016, of which 7.8% with an increasing trend and 14.4% with a decreasing trend (Fig. 2b), suggesting that disproportionate changes between vegetation greenness and productivity occurred in these areas. The strongest upward trends of EPE mainly appeared in eastern Brazil, clusters in the border area between Bolivia, Argentina and Paraguy, northern sub-Saharan Africa, eastern Africa (Somalia, Kenya and Tanzania), and clusters in southeastern China. While the downward trends of EPE are widely observed in eastern US, Scandinavia and eastern Europe, Siberia, India, southern China, southern Brazil, and central Africa (Fig. 2b).

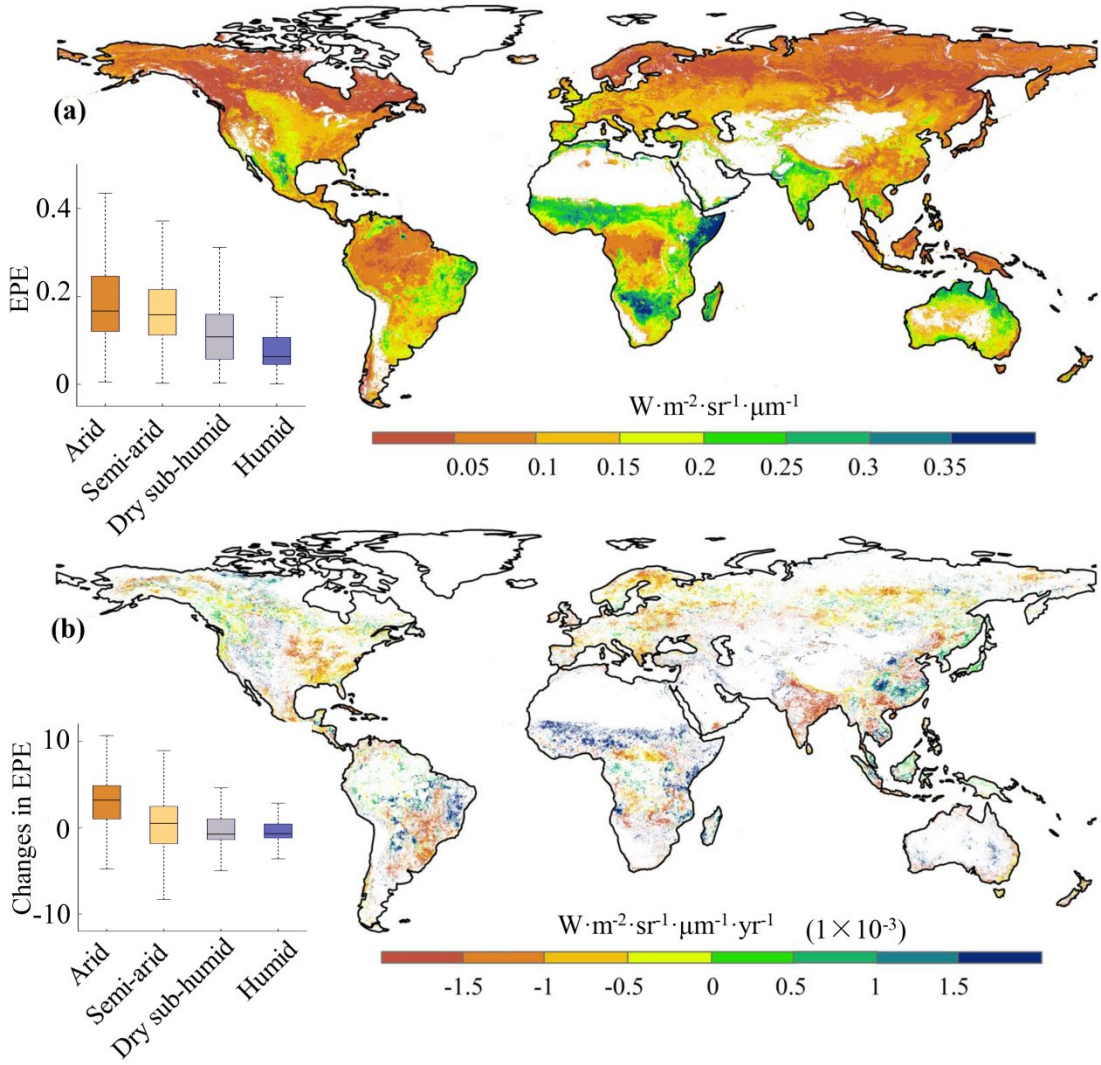


**Fig. 2.** The spatial patterns and temporal dynamics of ecosystem-scale photosynthetic efficiency (EPE) at a global scale. Maps of (a) the annual mean EPE and (b) significant ($p \leq 0.05$) changes in EPE during 2001-2016 (b). The inserted whisker plots were calculated for pixels in four different aridity zones. The lower and upper box edges correspond to the 25th and 75th percentiles, and the whiskers represent the 5th and 95th percentiles, respectively.

By overlaying the trends of EPE with the relative changes in SIF and LAI, we found that 76% of the areas with increasing EPE is caused by a larger increase in SIF than LAI, and the remaining 24% due to a smaller decrease in SIF than LAI (Fig. 3a, c). A smaller increase in SIF than LAI and a larger decrease in SIF than LAI explained 68% and 32% of the decreasing EPE, respectively (Fig. 3a, c). Those results suggest that the disproportionable increase of LAI and SIF dominated the significant changes in EPE. Moreover, we found the spatial pattern of relative changes

in SIF and LAI is consistent with relative changes in GPP and LAI in nearly 89% of areas (Fig. 3), confirming the robustness of our results. The inconsistent areas mainly located in densed forests, such as the Southeast Asia, where retrieving accurate vegetation indices from dense canopies and estimating the light use efficiency remain extremely challenging tasks.

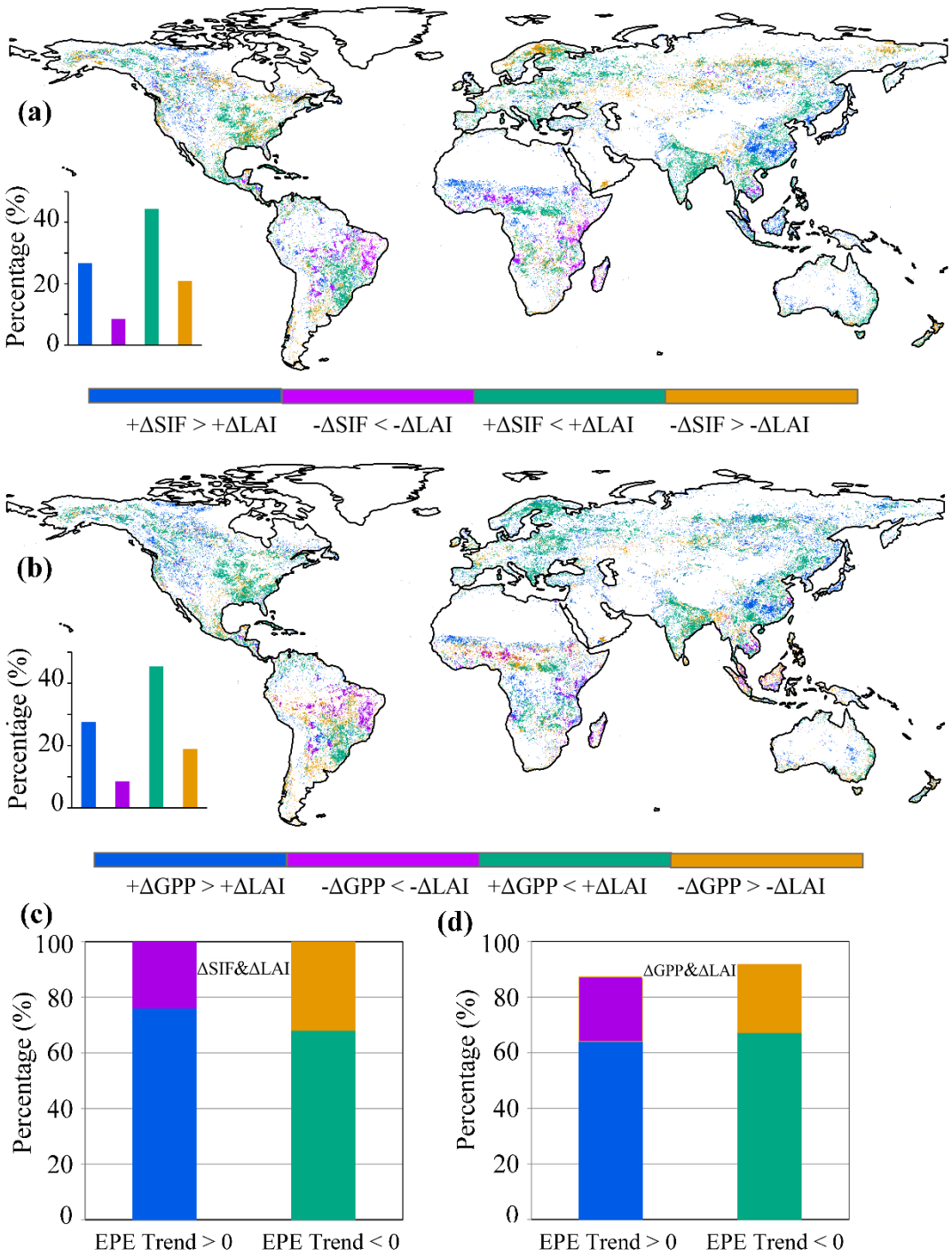


**Fig. 3.** Global distribution of the relative changes between vegetation productivity and

greenness. Comparison of relative changes in (a) SIF and LAI, (b) GPP and LAI during 2001-2016; percentages of pixels when overlaying EPE trends with relative changes in (c) SIF and LAI, (d) GPP and LAI.

## 3.2 EPE stratified by aridity gradients and land cover types

We subsequently investigated how annual mean EPE and changes in EPE varied along aridity gradients and among land cover types (Fig. 2& Fig. 4). Interestingly, we found that EPE increased with increasing aridity, with larger EPE in arid and semi-arid areas than dry sub-humid and humid regions (Fig. 2a). For the same land cover type, tropical vegetation has much higher EPE than extratropical vegetation, such as tropical shrublands (TSH) and extratropical shrublands (ESH), tropical savannas (TSA) and extratropical savannas (ESA), tropical grasslands (TGR) and extratropical grasslands (EGR, Fig. 4a). In addition, broadleaf vegetation has higher EPE than needleleaf vegetation (Fig. 4a).

The increasing trends of EPE dominated the arid (mean value of $2.6\times10^{-3}$ $W\cdot m^{-2}\cdot sr^{-1}\cdot \mu m^{-1}\ yr^{-1}$ or 1.6 % $yr^{-1}$) and semi-arid areas (mean value of $0.3\times10^{-3}$ $W\cdot m^{-2}\cdot sr^{-1}\cdot \mu m^{-1}\ yr^{-1}$ or 0.2 % $yr^{-1}$). In contrast, decreasing EPE trends were found in dry sub-humid (mean value of $-0.3\times10^{-3}$ $W\cdot m^{-2}\cdot sr^{-1}\cdot \mu m^{-1}\ yr^{-1}$ or -0.3 % $yr^{-1}$) and humid regions (mean value of $-0.5\times10^{-3}$ $W\cdot m^{-2}\cdot sr^{-1}\cdot \mu m^{-1}\ yr^{-1}$ or -0.4 % $yr^{-1}$) (Fig. 2b & Fig. S2a). These results are consistent with a stronger increase in SIF than in LAI in arid and semi-arid areas and a weaker increase in SIF than in LAI in dry sub-humid and humid regions (Fig. S2). Meanwhile, a positive trend of EPE was found in evergreen broadleaf forests, shrublands, and grasslands (Fig. 4b, c), in line with a higher increase in SIF than LAI in the above land cover types (Fig. S3 & Fig. S4). In contrast, the needleleaf forests, mixed forests, and crops experienced less increase in SIF than LAI (Fig. S3 & Fig. S4), supporting the negative trends of EPE in those land cover types (Fig. 4b, c). Areal statistics of trends in EPE for different aridity zones and land cover classes are shown in Tables. S1 and Table. S2, respectively.

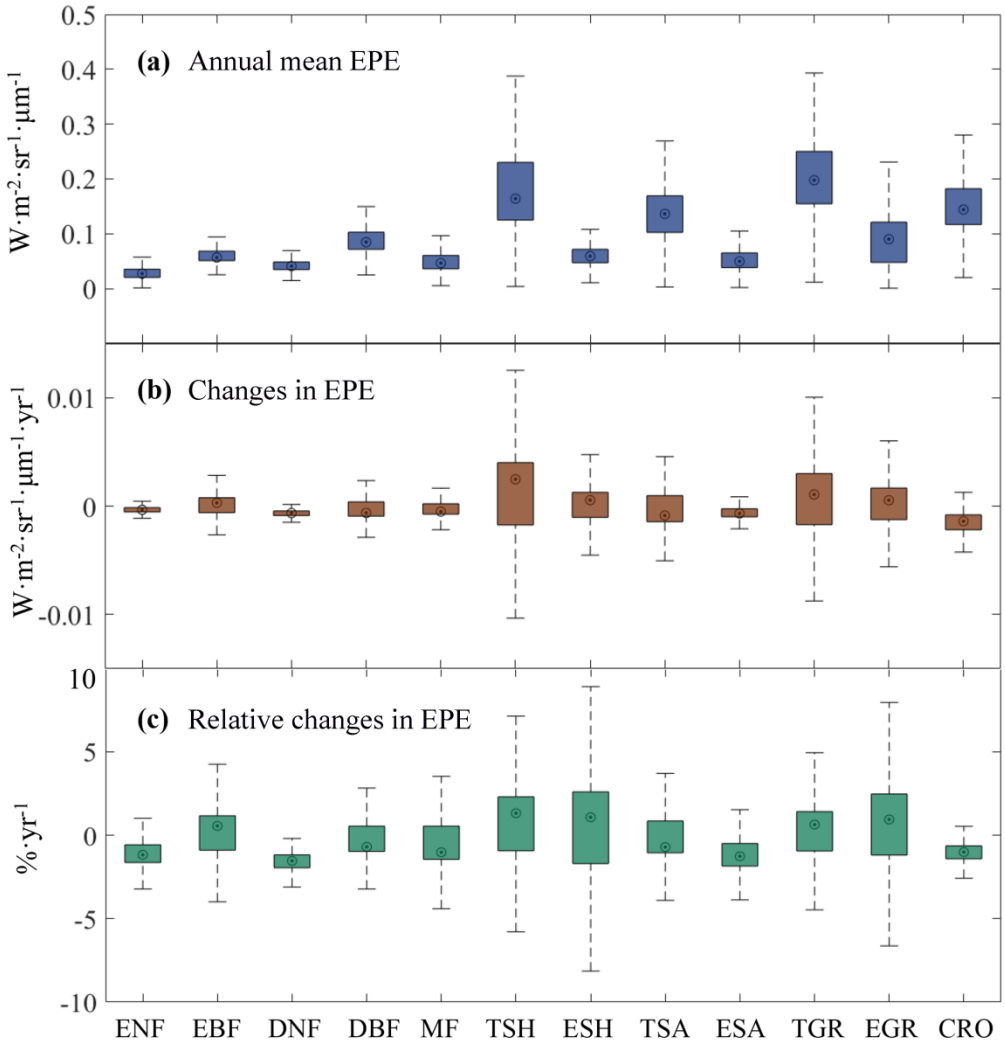


**Fig. 4.** The distribution of ecosystem-scale photosynthetic efficiency (EPE) and changes in EPE for each land cover class. (a) Annual mean value of EPE, (b) changes in SIF/LAI, and (c) relative changes in SIF/LAI during2001-2016. The lower and upper box edges correspond to the 25th and 75th percentiles, and the whiskers represent the 5th and 95th percentiles, respectively. ENF: evergreen needleleaf forest; EBF: evergreen broadleaf forest; DNF: deciduous needleleaf forest; DBF: deciduous broadleaf forest; MF: mixed forest; TSH: tropical shrublands; ESH: extratropical shrublands; TSA: tropical savannas; ESA: extratropical savannas; TGR: tropical grasslands; EGR: extratropical grasslands; CRO: croplands.

## 3.3 The responses of EPE to hydrometeorological factors and canopy structure

Many hydrometeorological factors affect the conversion of absorbed sunlight by

leaf to sequestered carbon, including solar radiation, minimum temperature, soil moisture, and water vapor pressure deficit (VPD). Canopy structure (e.g., the proportion of woody and grassy vegetation) also regulates the absorbed solar radiation by vegetation. Here we analyze the spatial dependence of EPE on hydrometeorological factors and canopy structure. The nonlinearity between SIF and GPP at small spatiotemporal scale due to the light saturation of GPP (i.e., GPP saturates at high light when SIF continues to increase) may lead to an artifact of EPE responding to solar radiation, yet studies have shown a near-linear relationship between SIF and GPP at large scales (Sun et al., 2018; Xiao et al., 2019). Thus, we performed the analysis on an annual scale based on satellite observations. The results showed that annual mean solar radiation (i.e., photosynthetically active radiation; PAR) positively affects EPE, with low EPE values in regions of low incoming radiation and high EPE values in regions of higher incoming radiation (Fig. 5a). Similarly, EPE positively responds to the minimum temperature ranging from -10°C to 10°C (Fig. 5b). Interestingly, we found contrary response modes of EPE to SM and VPD, with low values of EPE in mesic areas (i.e., high SM and low VPD) and high values of EPE in xeric areas (i.e., low SM and high VPD). This can be supported by the negative responses of EPE to precipitation and aridity index (Fig. S5a, b). It should be noted that these responses are nonlinear, for example, EPE is most sensitive to changes in SM from 0.2 $m^3 m^{-3}$ to 0.4 $m^3 m^{-3}$ and most sensitive to changes in VPD below 10 KPa (Fig. 3c, d). Additionally, EPE decreases with increasing vegetation cover (Fig. S5c), with high values of EPE in short vegetation dominated ecosystems and low values of EPE in tree dominated ecosystems (Fig. 5e, f). This is consistent with the response of EPE to canopy height that has a negative effect on EPE (Fig. S5d).

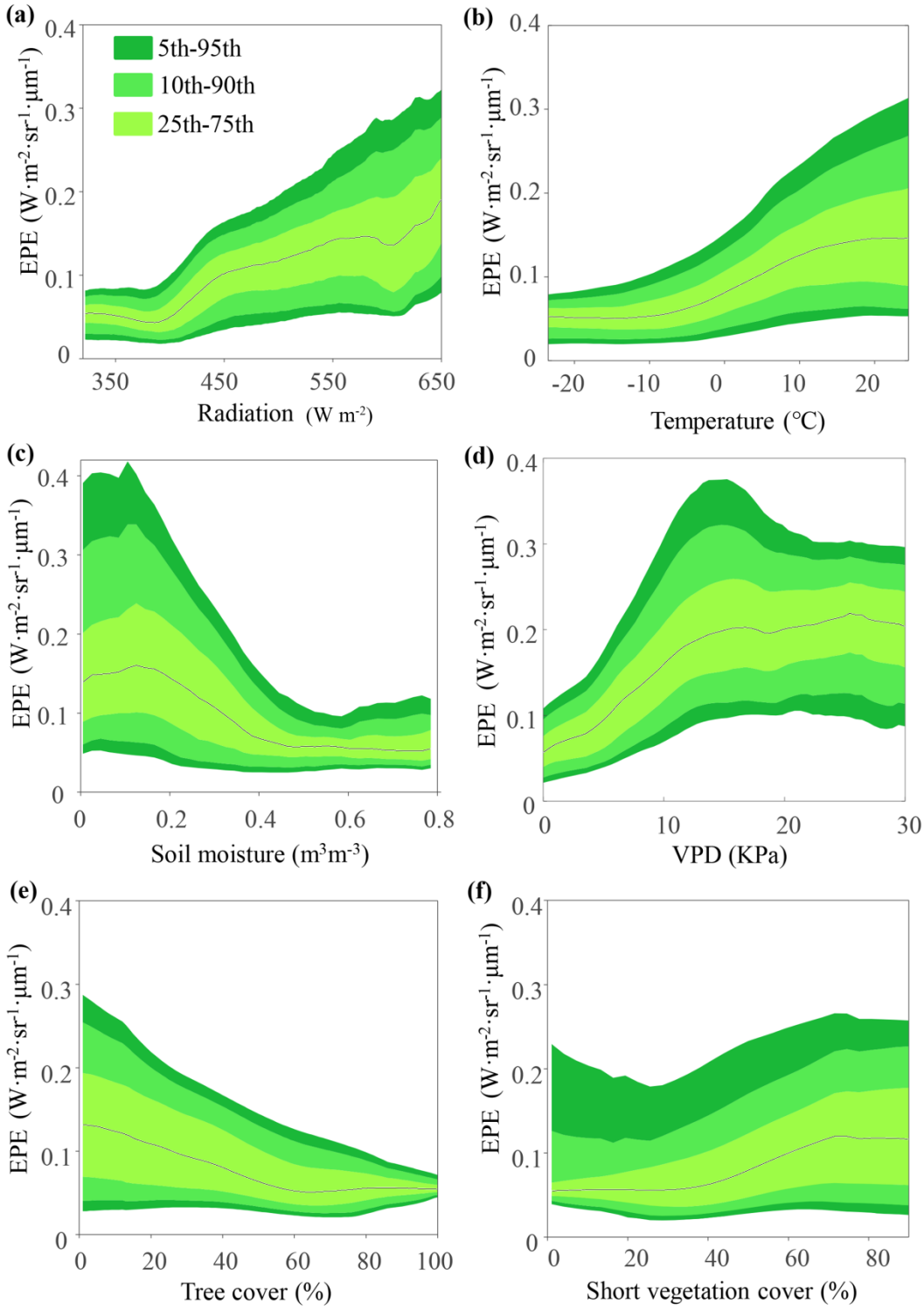


**Fig. 5.** The relationship between ecosystem-scale photosynthetic efficiency (EPE) and potential drivers during 2001-2016. (a) Radiation, (b) minimum temperature, (c) soil moisture, (d) water vapor pressure deficit (VPD), (e) tree cover, and (f) short vegetation cover. The black line denotes the median value.

We further explored the trends in potential factors controlling EPE. Solar radiation showed an upward trend among areas of different aridity classes (Fig. 6a), which

increased the active photosynthetic radiation. Minimum temperature also increased in each aridity zone (Fig. 6b), suggesting a general alleviation of low-temperature stress on EPE in global warming. Soil moisture overall increased except for the dry sub-humid areas with small negative trends (Fig. 6c), meaning a general relief of moisture stress on EPE from the perspective of water supply. VPD increased among areas of different aridity regions (Fig. 6d), suggesting an intensification of moisture stress on EPE from the perspective of atmospheric water demand. Moreover, we noticed that both short vegetation cover and tree cover increased in arid and semi-arid areas. Yet, the increase in short vegetation cover is at the expense of tree cover in dry sub-humid and humid regions (Fig. 6e, f). Therefore, the contributions of hydrometeorological factors and canopy structure to EPE should be further quantified to better understand the changes in EPE.

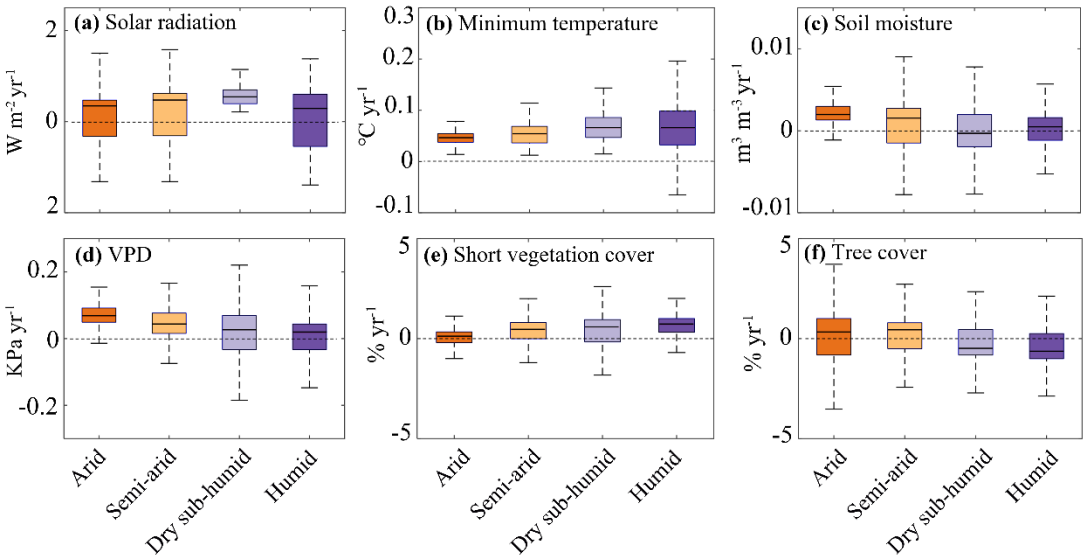


**Fig. 6.** Changes in factors affecting the ecosystem-scale photosynthetic efficiency (EPE) during 2001-2016. Box plots of the distribution of trends in (a) solar radiation, (b) minimum temperature, (c) soil moisture, (d) water vapor pressure deficit, (e) tree cover, and (f) short vegetation cover distributed by aridity zones. The maximum and minimum extents of the colored boxes indicate the 25th and 75th percentiles, and the whiskers represent the 5th and 95th percentiles, respectively.

## 3.4 Attribution of EPE to drivers

The relative contributions of the underlying factors controlling the observed changes in EPE were calculated for each grid cell by an empirical approach based on Principal Component Analysis (PCA) and Regression (PCR, see methods). We found

that most of the significant trends in EPE are primarily driven by changes in soil moisture (25%), followed by VPD (20%), temperature (19%), solar radiation (18%), and short vegetation cover (18%, Fig. 7a). The influence by SM is dominating across aridity zones, yet showing a pattern of decreasing importance along the aridity gradient (with the highest value of 43% in arid areas and lowest value of 22% in humid regions, Fig. 7b). In contrast, the percentage of pixels dominated by VPD increased along the aridity gradient (with the lowest value of 14% in arid areas and the highest value of 21% in humid regions, Fig. 7b). These results suggest that EPE is primarily controlled by soil moisture, yet the role of VPD is increasing with increasing humidity. We also found that areas dominated by solar radiation increased with increasing humidity, suggesting that EPE was constrained by radiation in relatively mesic ecosystems (Fig. 7b). Finally, short vegetation cover was found to be more dominating in xeric than in mesic regions, suggesting the critical role of canopy structure (e.g., the proportion of woody and grassy vegetation) on EPE in drylands (Fig. 7b). Tree cover was excluded from the analysis due to its close inverse relationship with short vegetation cover.

The sensitivity of changes in EPE to changes in driving factors was assessed based on the slope of PCR and the respective loadings from the PCA (see methods) (Fig. 7c). For arid areas, EPE changes were most sensitive to soil moisture changes, followed by short vegetation cover changes. However, in semi-arid ecosystems, EPE showed the highest sensitivity to short vegetation cover (Fig. 7c). Thus, changes in short vegetation cover can largely increase EPE in arid and semi-arid areas, whereas its role in explaining EPE trends in dry sub-humid and humid regions is limited. EPE was most sensitive to soil moisture in dry sub-humid and humid regions, followed by solar radiation. Interestingly, EPE was increased by soil moisture in arid and semi-arid areas, whereas it was decreased in dry sub-humid and humid regions. In contrast, solar radiation was found to affect EPE in mesic areas positively and negatively affect EPE in xeric areas. We noted that the sensitivities of EPE to VPD and minimum temperature were of opposite direction (negative for VPD and positive for minimum temperature) and almost of equal size for the different aridity zones (Fig. 7c).

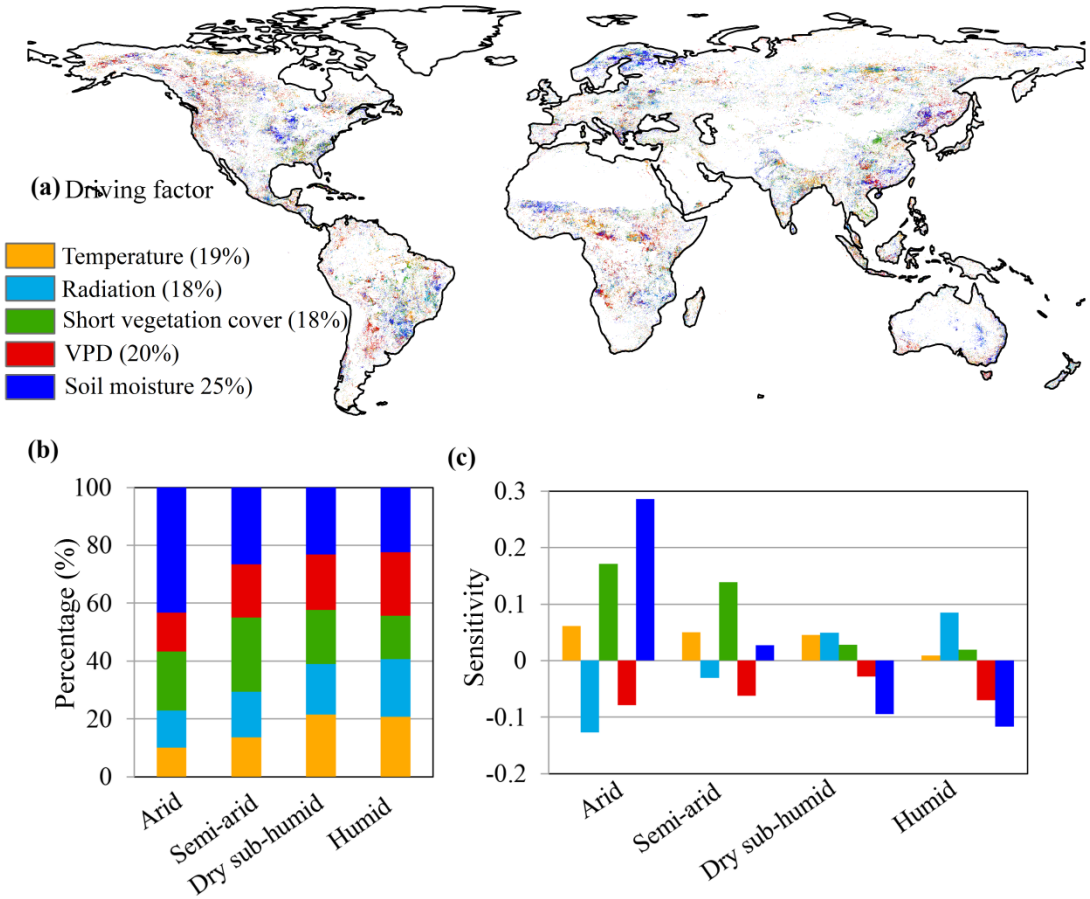


**Fig. 7.** Attribution of ecosystem-scale photosynthetic efficiency (EPE). (a) The driving factor that attributes the most to the increase (or decrease) in EPE indicated for each grid cell, (b) the area fractions of land dominated by each factor in different aridity zones, and (c) sensitivity of changes in EPE towards changes in these driving factors for different aridity zones.

# 4. Discussion

Previous studies have reported widespread greening and increased ecosystem productivity over recent decades (Chen et al., 2019a; Huang et al., 2018; Piao et al., 2019), yet how this substantial greening is linked with the ecosystem productivity increase is not clear. Our results reported a weaker increase in productivity (0.43% $yr^{-1}$ for SIF) comparing with the global greening rate (0.63% $yr^{-1}$ for LAI) during 2001-2016, suggesting a decline in EPE globally. When stratified by areas with different aridity, we found a stronger increase in productivity than greenness in arid and semi-arid areas (0.82% $yr^{-1}$ for SIF and 0.57% $yr^{-1}$ for LAI), yet a weaker increase in productivity than greenness in dry sub-humid and humid regions (0.36% $yr^{-1}$ for

SIF and 0.64% $yr^{-1}$ LAI, Fig. S6). These results are consistent with the EPE trends in different aridity classes (i.e., with upward trends in arid and semi-arid areas and downward trends in dry sub-humid and humid regions), suggesting that arid and semi-arid areas (i.e., xeric ecosystems) contribute more to the global productivity increase than to the Earth greening, and vice versa for dry sub-humid and humid regions (i.e., mesic ecosystems).

The above results based on GOSIF and GLOBMAP LAI showed a good consistency compared with CSIF and SPOT LAI (Fig. S6), suggesting the robustness of our results. However, we must acknowledge that uncertainties in EPE estimation resulted from potential errors in both SIF and LAI datasets. To give uncertainty information, we calculated the EPE using different combinations of datasets (i.e., GOSIF and GLOBMAP LAI, CSIF and GLOBMAP LAI, GOSIF and SPOT LAI, and CSIF and SPOT LAI) and analyzed the spatio-temporal patterns correspondingly (Fig. S7, 8). The results showed that the spatial pattern of EPE among different combinations of datasets matched well, with higher EPE in arid areas than in humid regions (Fig. S7). We also found the EPE trends among different combinations of datasets were comparable (Fig. S8). However, due to GLOBMAP LAI is smaller than SPOT LAI, $EPE_{GG}$ and $EPE_{CG}$ are overall larger than $EPE_{GS}$ and $EPE_{CS}$ (Fig. S7). The magnitudes of $EPE_{GG}$ trends and $EPE_{CG}$ trends are overall larger than $EPE_{GS}$ trends and $EPE_{CS}$ trends (Fig. S8), particularly for drylands in Africa with large uncertainty (i.e., large standard deviation of EPE or EPE trends). Moreover, satellite observations in tropical forests are highly uncertain due to higher cloud optical thickness, water vapor contents, and less well-known aerosol properties, where retrieving accurate LAI or SIF is more challenging (Ryu et al., 2019). In our study, a large part of the tropics, particularly the rainforests, showed insignificant changes in EPE (Fig. 2b). The possible reason is that the large interannual variations, such as responses to drought, have hidden the long-term trends. In fact, the interannual variations in greenness and photosynthesis could also be decoupled, for example, Amazonian forests experienced a significant decrease in photosynthesis but a slight increase in vegetation greenness after an extreme drought event in 2015/2016 (Yang et al., 2018), indicating that

rainforest photosynthesis could still be suppressed regardless of the variation in canopy greenness. If more frequent and intense droughts in the future as projected by earth system models, tropical forests will experience a persistent reduction in EPE.

Moreover, we found that the EPE increased most in natural short vegetation (i.e., shrublands and grasslands, Fig. 4b, c), where a higher increasing productivity than vegetation greenness was also observed (Fig. S4). However, forests (except evergreen broadleaf forest) and croplands showed a lower productivity increase than greenness (Fig. S4), which is in line with a decreasing EPE trend (Fig. 4b, c). A recent study confirmed that the Earth greening overlaps with global major forests and croplands and is strikingly prominent in the two most populous countries on Earth – China and India (Chen et al., 2019a). However, the current greening in human-managed ecosystems is at the cost of decreasing EPE, where the carbon sequestration is limited and does not increase proportionally. These results underscore that using vegetation greenness as a proxy for productivity may overestimate or underestimate the regional ecosystem carbon sink. Overall, the nonlinearity between SIF and LAI can be well represented by EPE, which directly affects the EPE trends. This is due to the light saturation effect that as LAI gets higher, light absorption/photosynthesis for each leaf decreases (Marrs et al., 2020; Pierrat et al., 2022), and so is EPE. Our study reveals a spatially disproportionate increase in ecosystem productivity against the widespread notion of a greening Earth.

What factors regulate the relationship between vegetation greenness and productivity? A recent study reported that the increase in LAI alone was responsible for 12.4% of the accumulated carbon sink (Chen et al., 2019b). Besides the leaf quantity (amount of leaf area or LAI), photosynthetic capacity is affected by leaf quality (the photosynthetic rate of each individual leaf) (Wu et al., 2016; Zhang et al., 2017). The leaf quality is mostly related to the leaf chlorophyll content and the leaf nitrogen content (Kattge et al., 2009). Ecosystem productivity is also affected by hydrometeorological factors (Fig. 5). $CO_2$ fertilization can promote carbon sequestration by enhancing the water use efficiency of plants (Lu et al., 2016), yet which has declined due to the emerging nutrient constraints (Peñuelas et al., 2017;

Wang et al., 2020). Additionally, studies reported that productivity is more sensitive to environmental changes than greenness, and productivity can vary at a much higher frequency relative to greenness mediated by leaf chlorophyll content and canopy structure (Smith et al., 2018; Yan et al., 2019). Thus, it is not surprising that the relationship of vegetation greenness-productivity varies in both time and space.

The results showed that the restriction of minimum temperature on EPE has weakened as a function of global warming. Plants' water stress is controlled by soil water supply and atmospheric water demand, coupled through land-atmosphere interactions (Stocker et al., 2018, Lian et al., 2021). Here we found overall increases in soil moisture and atmospheric drought (Fig. 6c, d). VPD showed negative effects on EPE (Fig. 7c). Yet, the negative effect of increasing VPD on EPE was offset by a positive impact from increasing soil moisture in arid and semi-arid areas. In contrast, soil moisture showed adverse effects on EPE in dry sub-humid and humid regions, which exacerbated the negative effects of VPD (Fig. 7c). Thus, adverse effects of high soil moisture on EPE should be given equal attention to soil drought stress in the future. EPE was primarily controlled by soil moisture (Fig. 7), consistent with recent studies that reported that soil moisture dominates dryness stress on global ecosystem production (Feng et al., 2021; Liu et al., 2020; Stocker et al., 2018). Additionally, EPE positively responds to the increase in short vegetation cover in arid and semi-arid areas, yet the role of which is limited in dry sub-humid and humid regions (Fig. 7b, c). Thus, there is no surprise that EPE showed upward and downward trends in relatively xeric and mesic ecosystems, respectively. Such distinctions in ecological strategies between xeric and mesic ecosystems are crucial for understanding the complex effects of climatic stress on EPE (Migliavacca et al., 2021).

# 5. Conclusion

This study defined a new metric of ecosystem-scale photosynthetic efficiency (EPE), uncovered the spatial pattern and dynamics of EPE, and analyzed its driving mechanisms better to understand climate change impacts on ecosystem structure and

function. EPE well links ecosystem productivity with greenness and thus helps investigate how potential factors regulate the vegetation greenness-productivity relationship. Our study reported a decline in EPE globally, suggesting that the current carbon sequestration rate does not increase proportionally to Earth's greening. Moreover, the spatiotemporal pattern of EPE and its drivers showed spatial heteorogenity: EPE overall showed upward trends in arid and semi-arid areas (i.e., xeric ecosystems) and downward trends in dry sub-humid and humid regions (i.e., mesic ecosystems). The EPE was primarily controlled by soil moisture that promoted and constrained the EPE in xeric and mesic ecosystems, respectively. Meanwhile, short vegetation cover positively contributed to EPE in xeric ecosystems, while atmospheric water demand negatively correlated with EPE in mesic ecosystems. The knowledge gained by introducing EPE can improve our understanding of simulations and predictions of the terrestrial ecosystem carbon cycle, reducing the uncertainties of future climate change predictions and guiding policymaking for sustainable ecosystem management.

## Data availability

The GOSIF data is available at http://data.globalecology.unh.edu/data/GOSIF_v2/. The CSIF can be downloaded from https://doi.org/10.6084/m9.figshare.6387494. The global GLOBMAPV3 LAI dataset can be downloaded at http://globalmapping.org/globalLAI/. The SPOT LAI can be derived from https://land.copernicus.eu/global/products/lai. The MODIS VCF data can be derived from https://doi.org/10.5067/MODIS/MOD44B.006. The CRU minimum and mean temperature is available at https://crudata.uea.ac.uk/cru/data/hrg/. The CERES PAR data can be downloaded from https://ceres.larc.nasa.gov/order_data.php. The GLEAM soil moisture data is available at https://www.gleam.eu/. The ERA relative humidity is available at https://www.ecmwf.int/en/forecasts/datasets/reanalysis-datasets/era-interim. The Global thermal climate zone map derived from http://www.fao.org/geonetwork/srv/en/metadata.show?id=14056&currTab=simple. The MODIS land cover data is available at https://lpdaac.usgs.gov/products/mcd12q1v006/#tools.

Aridity index data is available at https://cgiarcsi.community/2019/01/24/global-aridity-index-and-potential-evapotranspiration-climate-database-v2/.

## References


Abel, C., Horion, S., Tagesson, T., De Keersmaecker, W., Seddon, A.W.R., Abdi, A.M., Fensholt, R. (2020) The human–environment nexus and vegetation–rainfall sensitivity in tropical drylands. Nature Sustainability 4, 25-32.

Berrisford, P., Dee, D., Poli, P., Brugge, R., Fielding, K., Fuentes, M., Kållberg, P., Kobayashi, S., Uppala, S., Simmons, A. (2011) The ERA-Interim archive Version 2.0, Shinfield Park. Reading 1, 23.

Bronaugh, D., Werner, A. (2013) Zhang + Yue-Pilon trends package. R Package Version 0.10-1.[Available online at https://cran. r-project. org/web/packages/zyp/index. html.].

Chen, C., Park, T., Wang, X., Piao, S., Xu, B., Chaturvedi, R.K., Fuchs, R., Brovkin, V., Ciais, P., Fensholt, R. (2019a) China and India lead in greening of the world through land-use management. Nature Sustainability 2, 122-129.

Chen, J.M., Ju, W., Ciais, P., Viovy, N., Liu, R., Liu, Y., Lu, X. (2019b) Vegetation structural change since 1981 significantly enhanced the terrestrial carbon sink. Nature communications 10, 1-7.

Ammann, C. & Schaepman, M.E. (2015) Far-red sun-induced chlorophyll fluorescence shows ecosystem-specific relationships to gross primary production: An assessment based on observational and modeling approaches. Remote Sensing of Environment 166, 91-105.

Deng, F., Chen, J.M., Plummer, S., Chen, M., Pisek, J. (2006) Algorithm for global leaf area index retrieval using satellite imagery. Ieee Transactions on Geoscience and Remote Sensing 44, 2219-2229.

Detsch, F., Otte, I., Appelhans, T., Hemp, A., Nauss, T. (2016) Seasonal and long-term vegetation dynamics from 1-km GIMMS-based NDVI time series at Mt. Kilimanjaro, Tanzania. Remote Sensing of Environment 178, 70-83.

Feng, X., Fu, B., Zhang, Y., Pan, N., Zeng, Z., Tian, H., Lyu, Y., Chen, Y., Ciais, P. & Wang, Y.

(2021) Recent leveling off of vegetation greenness and primary production reveals the increasing soil water limitations on the greening Earth. Science Bulletin, 66, 1462-1471.

Forzieri, G., Alkama, R., Miralles, D.G., Cescatti, A. (2017) Satellites reveal contrasting responses of regional climate to the widespread greening of Earth. Science 356, 1180-1184.

Frankenberg, C., Fisher, J.B., Worden, J., Badgley, G., Saatchi, S.S., Lee, J.E., Toon, G.C., Butz, A., Jung, M., Kuze, A. (2011) New global observations of the terrestrial carbon cycle from GOSAT: Patterns of plant fluorescence with gross primary productivity. Geophysical Research Letters 38.

Hamed, K.H., Rao, A.R. (1998) A modified Mann-Kendall trend test for autocorrelated data. Journal of hydrology 204, 182-196.

Huang, K., Xia, J., Wang, Y., Ahlstrom, A., Chen, J., Cook, R.B., Cui, E., Fang, Y., Fisher, J.B., Huntzinger, D.N., Li, Z., Michalak, A.M., Qiao, Y., Schaefer, K., Schwalm, C., Wang, J., Wei, Y., Xu, X., Yan, L., Bian, C., Luo, Y. (2018) Enhanced peak growth of global vegetation and its key mechanisms. Nature Ecology & Evolution 2, 1897-1905.

Joiner, J., Yoshida, Y., Vasilkov, A., Middleton, E. (2011) First observations of global and seasonal terrestrial chlorophyll fluorescence from space. Biogeosciences 8, 637-651.

Jones, P. (2019) CRU TS4. 03: Climatic Research Unit (CRU) Time-Series (TS) Version 4.03 of High-Resolution Gridded Data of Month-by-Month Variation in Climate (January 1901–December 2018). CEDA: Didcot, UK.

Kattge, J., Knorr, W., Raddatz, T., Wirth, C. (2009) Quantifying photosynthetic capacity and its relationship to leaf nitrogen content for global-scale terrestrial biosphere models. Global Change Biology 15, 976-991.

Kaufmann, M.R., Troendle, C.A. (1981) The relationship of leaf area and foliage biomass to sapwood conducting area in four subalpine forest tree species. Forest Science 27, 477-482.

Li, X., Xiao, J. (2019) A global, 0.05-degree product of solar-induced chlorophyll fluorescence derived from OCO-2, MODIS, and reanalysis data. Remote Sensing 11, 517.

Lian, X., Piao, S., Chen, A., Huntingford, C., Fu, B., Li, L.Z., Huang, J., Sheffield, J., Berg, A.M., Keenan, T.F. (2021) Multifaceted characteristics of dryland aridity changes in a warming world. Nature Reviews Earth & Environment 2, 232-250.

Liu, X., Feng, X., Fu, B. (2020) Changes in global terrestrial ecosystem water use efficiency

are closely related to soil moisture. Science of The Total Environment 698, 134165.

Lu, X., Wang, L., McCabe, M.F. (2016) Elevated $CO_2$ as a driver of global dryland greening. Scientific Reports 6, 1-7.

Marrs, J., Reblin, J., Logan, B., Allen, D., Reinmann, A., Bombard, D., Tabachnik, D. & Hutyra, L. (2020) Solar‐induced fluorescence does not track photosynthetic carbon assimilation following induced stomatal closure. Geophysical Research Letters, 47, e2020GL087956.

McNally, A., Arsenault, K., Kumar, S., Shukla, S., Peterson, P., Wang, S., Funk, C., Peters-Lidard, C.D., Verdin, J.P. (2017) A land data assimilation system for sub-Saharan Africa food and water security applications. Scientific Data 4, 170012.

Middleton, N. (1997) World atlas of desertification.. ed. 2.

Migliavacca, M., Musavi, T., Mahecha, M.D., Nelson, J.A., Knauer, J., Baldocchi, D.D., Perez-Priego, O., Christiansen, R., Peters, J., Anderson, K. (2021) The three major axes of terrestrial ecosystem function. Nature, 1-5.

Peñuelas, J., Ciais, P., Canadell, J.G., Janssens, I.A., Fernández-Martínez, M., Carnicer, J., Obersteiner, M., Piao, S., Vautard, R., Sardans, J. (2017) Shifting from a fertilization-dominated to a warming-dominated period. Nature Ecology & Evolution 1, 1438-1445.

Pettorelli, N., Vik, J.O., Mysterud, A., Gaillard, J.M., Tucker, C.J., Stenseth, N.C. (2005) Using the satellite-derived NDVI to assess ecological responses to environmental change. Trends in Ecology & Evolution 20, 503-510.

Piao, S., Wang, X., Park, T., Chen, C., Lian, X., He, Y., Bjerke, J.W., Chen, A., Ciais, P., Tømmervik, H. (2019) Characteristics, drivers and feedbacks of global greening. Nature Reviews Earth & Environment, 1-14.

Pierrat, Z., Magney, T., Parazoo, N.C., Grossmann, K., Bowling, D.R., Seibt, U., Johnson, B., Helgason, W., Barr, A. & Bortnik, J. (2022) Diurnal and Seasonal Dynamics of Solar‐Induced Chlorophyll Fluorescence, Vegetation Indices, and Gross Primary Productivity in the Boreal Forest. Journal of Geophysical Research: Biogeosciences, 127, e2021JG006588.

Poulter, B., Frank, D., Ciais, P., Myneni, R.B., Andela, N., Bi, J., Broquet, G., Canadell, J.G., Chevallier, F., Liu, Y.Y., Running, S.W., Sitch, S., van der Werf, G.R. (2014) Contribution of

semi-arid ecosystems to interannual variability of the global carbon cycle. Nature 509, 600-603.

Ryu, Y., Berry, J.A., Baldocchi, D.D. (2019) What is global photosynthesis? History, uncertainties and opportunities. Remote Sensing of Environment 223, 95-114.

Smith, W.K., Biederman, J.A., Scott, R.L., Moore, D.J.P., He, M., Kimball, J.S., Yan, D., Hudson, A., Barnes, M.L., MacBean, N., Fox, A.M., Litvak, M.E. (2018) Chlorophyll Fluorescence Better Captures Seasonal and Interannual Gross Primary Productivity Dynamics Across Dryland Ecosystems of Southwestern North America. Geophysical Research Letters 45, 748-757.

Stocker, B.D., Zscheischler, J., Keenan, T.F., Prentice, I.C., Peñuelas, J., Seneviratne, S.I. (2018) Quantifying soil moisture impacts on light use efficiency across biomes. New Phytologist 218, 1430-1449.

Sulla-Menashe, D., Friedl, M.A. (2018) User guide to collection 6 MODIS land cover (MCD12Q1 and MCD12C1) product. USGS: Reston, VA, USA, 1-18.

Sun, Y., Frankenberg, C., Jung, M., Joiner, J., Guanter, L., Köhler, P., Magney, T. (2018) Overview of Solar-Induced chlorophyll Fluorescence (SIF) from the Orbiting Carbon Observatory-2: Retrieval, cross-mission comparison, and global monitoring for GPP. Remote Sensing of Environment 209, 808-823.

Walther, S., Voigt, M., Thum, T., Gonsamo, A., Zhang, Y., Kohler, P., Jung, M., Varlagin, A. & Guanter, L. (2016) Satellite chlorophyll fluorescence measurements reveal large-scale decoupling of photosynthesis and greenness dynamics in boreal evergreen forests. Glob Chang Biol, 22, 2979-96.

Wang, J., Xiao, X., Wagle, P., Ma, S., Baldocchi, D., Carrara, A., Zhang, Y., Dong, J., Qin, Y. (2016) Canopy and climate controls of gross primary production of Mediterranean-type deciduous and evergreen oak savannas. Agricultural and Forest Meteorology 226, 132-147.

Wang, S., Zhang, Y., Ju, W., Chen, J.M., Ciais, P., Cescatti, A., Sardans, J., Janssens, I.A., Wu, M., Berry, J.A. (2020) Recent global decline of $CO_2$ fertilization effects on vegetation photosynthesis. Science 370, 1295-1300.

Wielicki, Bruce, A., Barkstrom, Bruce, R., Harrison, Edwin, F., Lee (1996) Clouds and the Earth's Radiant Energy System (CERES): An Earth Observing System Experiment.

Bull.amer.meteor.soc 77, 853-868.

Wu, J., Albert, L.P., Lopes, A.P., Restrepo-Coupe, N., Hayek, M., Wiedemann, K.T., Guan, K., Stark, S.C., Christoffersen, B., Prohaska, N. (2016) Leaf development and demography explain photosynthetic seasonality in Amazon evergreen forests. Science 351, 972-976.

Xiao, J., Li, X., He, B., Arain, M.A., Beringer, J., Desai, A.R., Emmel, C., Hollinger, D.Y., Krasnova, A., Mammarella, I. (2019) Solar-induced chlorophyll fluorescence exhibits a universal relationship with gross primary productivity across a wide variety of biomes. Global Change Biology 25, e4-e6.

Yan, D., Scott, R.L., Moore, D.J.P., Biederman, J.A., Smith, W.K. (2019) Understanding the relationship between vegetation greenness and productivity across dryland ecosystems through the integration of PhenoCam, satellite, and eddy covariance data. Remote Sensing of Environment 223, 50-62.

Yang, J., Tian, H., Pan, S., Chen, G., Zhang, B., Dangal, S. (2018) Amazon drought and forest response: Largely reduced forest photosynthesis but slightly increased canopy greenness during the extreme drought of 2015/2016. Global Change Biology 24, 1919-1934.

Yuan, W.P., Zheng, Y., Piao, S.L., Ciais, P., Lombardozzi, D., Wang, Y.P., Ryu, Y., Chen, G.X., Dong, W.J., Hu, Z.M., Jain, A.K., Jiang, C.Y., Kato, E., Li, S.H., Lienert, S., Liu, S.G., Nabel, J.E.M.S., Qin, Z.C., Quine, T., Sitch, S., Smith, W.K., Wang, F., Wu, C.Y., Xiao, Z.Q., Yang, S. (2019) Increased atmospheric vapor pressure deficit reduces global vegetation growth. Science Advances 5, eaax1396.

Zhang, Y., Xiao, X., Wu, X., Zhou, S., Zhang, G., Qin, Y., Dong, J. (2017) A global moderate resolution dataset of gross primary production of vegetation for 2000–2016. Scientific data 4, 1-13.

Zhu, Z.C., Piao, S.L., Myneni, R.B., Huang, M.T., Zeng, Z.Z., Canadell, J.G., Ciais, P., Sitch, S., Friedlingstein, P., Arneth, A., Cao, C.X., Cheng, L., Kato, E., Koven, C., Li, Y., Lian, X., Liu, Y.W., Liu, R.G., Mao, J.F., Pan, Y.Z., Peng, S.S., Penuelas, J., Poulter, B., Pugh, T.A.M., Stocker, B.D., Viovy, N., Wang, X.H., Wang, Y.P., Xiao, Z.Q., Yang, H., Zaehle, S., Zeng, N. (2016) Greening of the Earth and its drivers. Nature Climate Change 6, 791-796.

# Figure legends

**Fig. 1.** Global distribution of aridity classes and land-cover types.

**Fig. 2.** The spatial patterns and temporal dynamics of ecosystem-scale photosynthetic efficiency (EPE) at a global scale.

**Fig. 3.** Global distribution of the relative changes between vegetation productivity and greenness.

**Fig. 4.** The distribution of ecosystem-scale photosynthetic efficiency (EPE) and changes in EPE for each land cover class.

**Fig. 5.** The relationship between ecosystem-scale photosynthetic efficiency (EPE) and potential drivers during 2001-2016.

**Fig. 6.** Changes in factors affecting the ecosystem-scale photosynthetic efficiency (EPE) during 2001-2016.

**Fig. 7.** Attribution of ecosystem-scale photosynthetic efficiency (EPE).

# Supplementary material

## Figure legends

**Fig. S1.** Global pattern of changes in vegetation greenness and productivity.

**Fig. S2.** Distribution of changes in LAI and SIF for different aridity zones.

**Fig. S3.** Changes in vegetation greenness and productivity per land cover class.

**Fig. S4.** Relative changes in vegetation greenness and productivity per land cover class.

**Fig. S5.** Spatial relationships between ecosystem-scale photosynthetic efficiency (EPE) and potential drivers during 2001-2016.

**Fig. S6.** Time series and linear trends of SIF and LAI during 2001-2016.

**Fig. S7.** Global pattern of ecosystem-scale photosynthetic efficiency (EPE) during 2001-2016.

**Fig. S8.** Temporal dynamics of ecosystem-scale photosynthetic efficiency (EPE) during 2001-2016.

## Table legends

**Table. S1.** Statistics of trends in ecosystem-scale photosynthetic efficiency (EPE) for different aridity classes.

**Table. S2.** Statistics of trends in ecosystem-scale photosynthetic efficiency (EPE) for each land cover class.

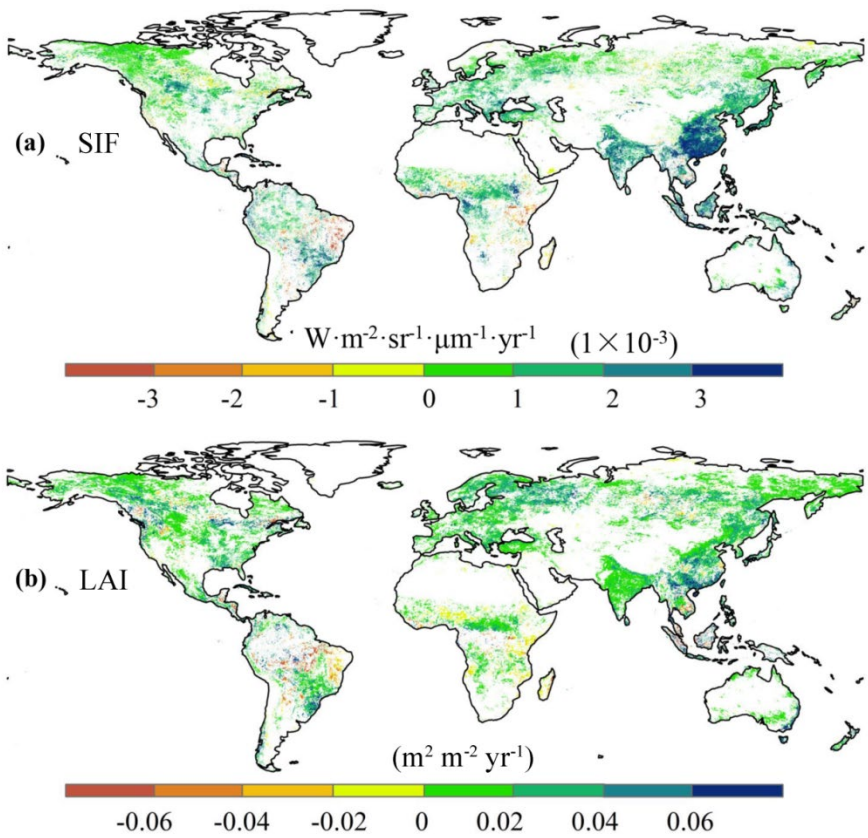


**Fig. S1.** Global pattern of changes in vegetation greenness and productivity. (a) solar-induced chlorophyll fluorescence (SIF) and (b) leaf area index (LAI) during 2001-2016.

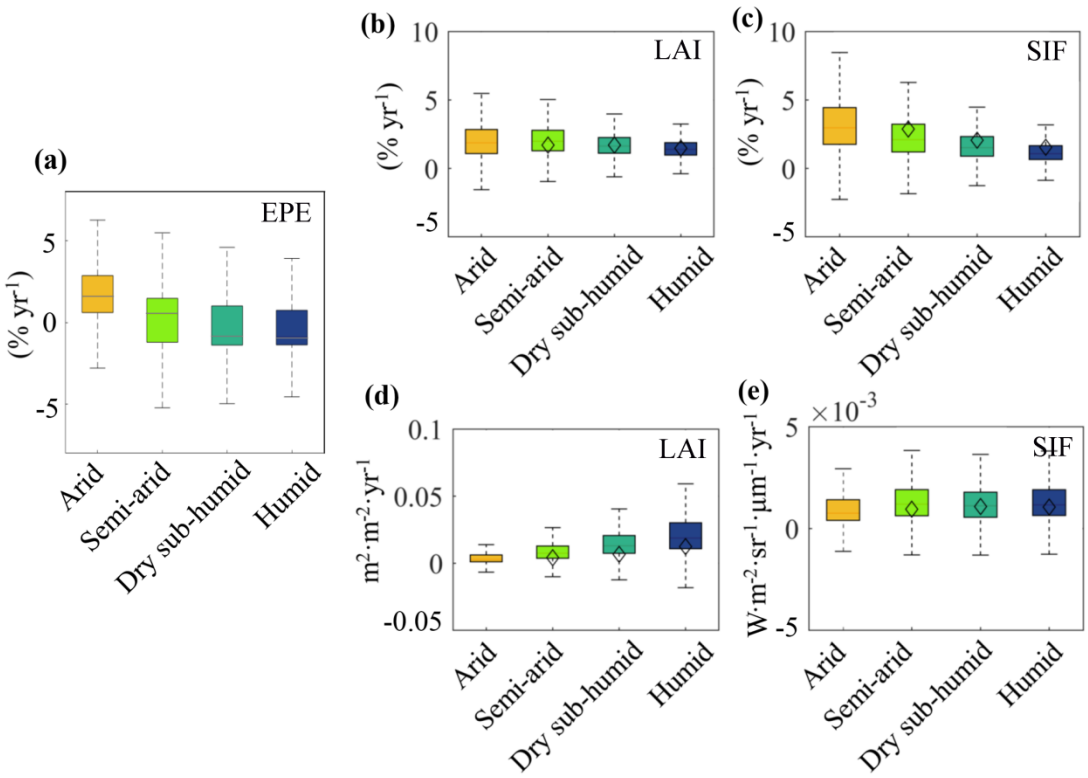


**Fig. S2.** Distribution of changes in LAI and SIF for different aridity zones. Relative changes in (a) ecosystem-scale photosynthetic efficiency (EPE), (b) LAI, and (c) SIF, changes in (d) LAI and (e) SIF. The lower and upper box edges correspond to the 25th and 75th percentiles, and the whiskers represent the 5th and 95th percentiles, respectively.

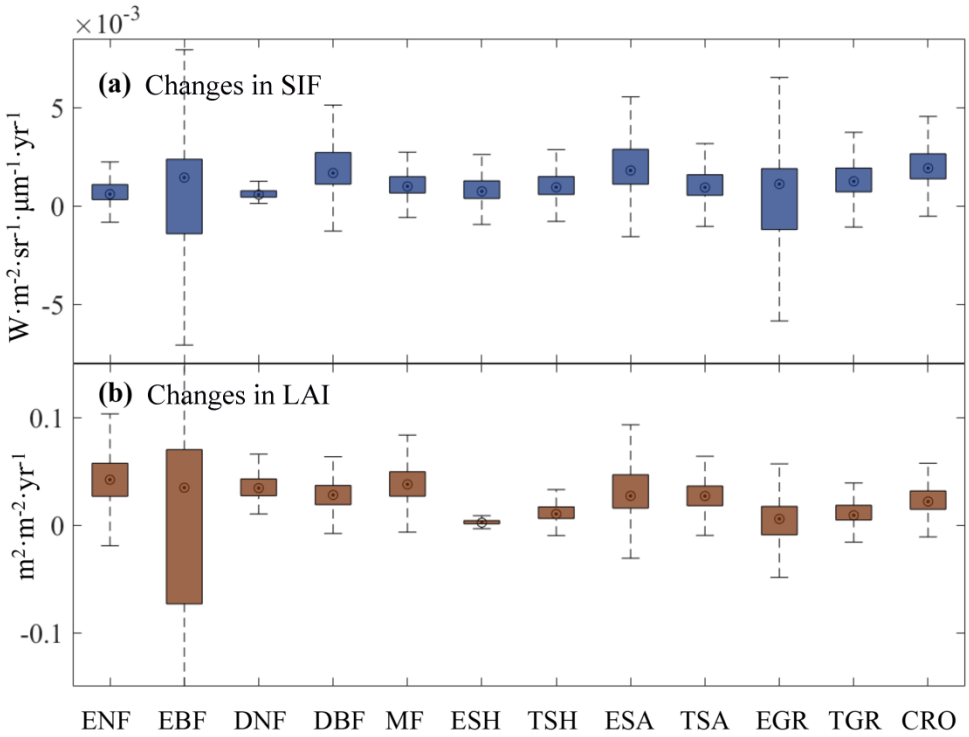


**Fig. S3.** Changes in vegetation greenness and productivity per land cover class. Changes in (a) SIF and (b) LAI. The lower and upper box edges correspond to the 25th and 75th percentiles, and the whiskers represent the 5th and 95th percentiles, respectively.

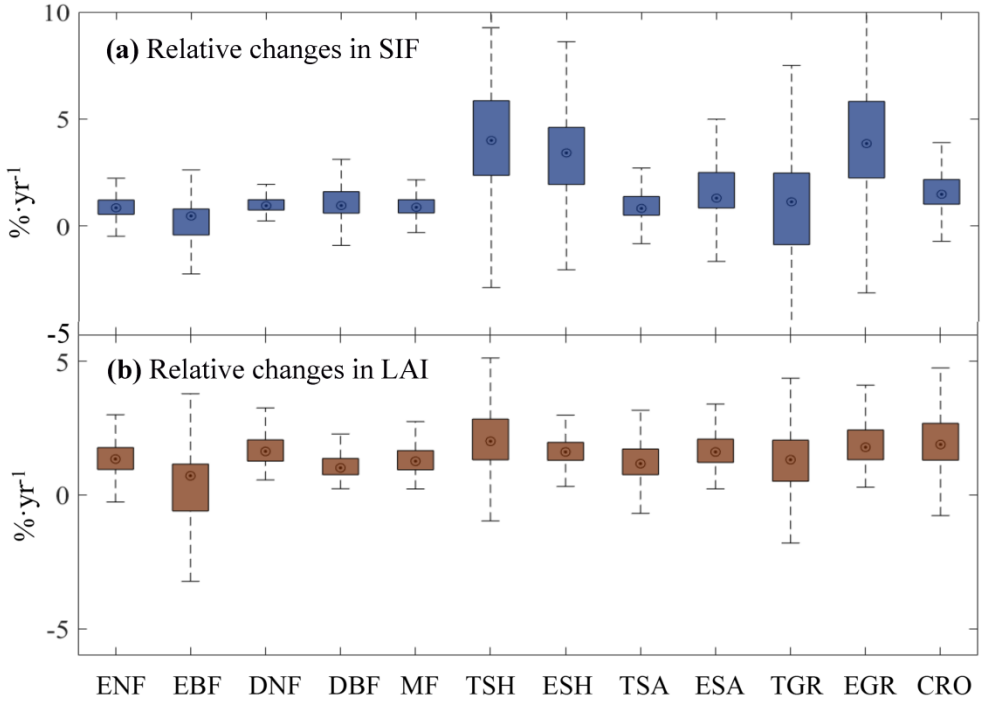


**Fig. S4.** Relative changes in vegetation greenness and productivity per land cover class. Relative changes in (a) SIF and (b) LAI. The lower and upper box edges correspond to the 25th and 75th percentiles, and the whiskers represent the 5th and 95th percentiles, respectively.

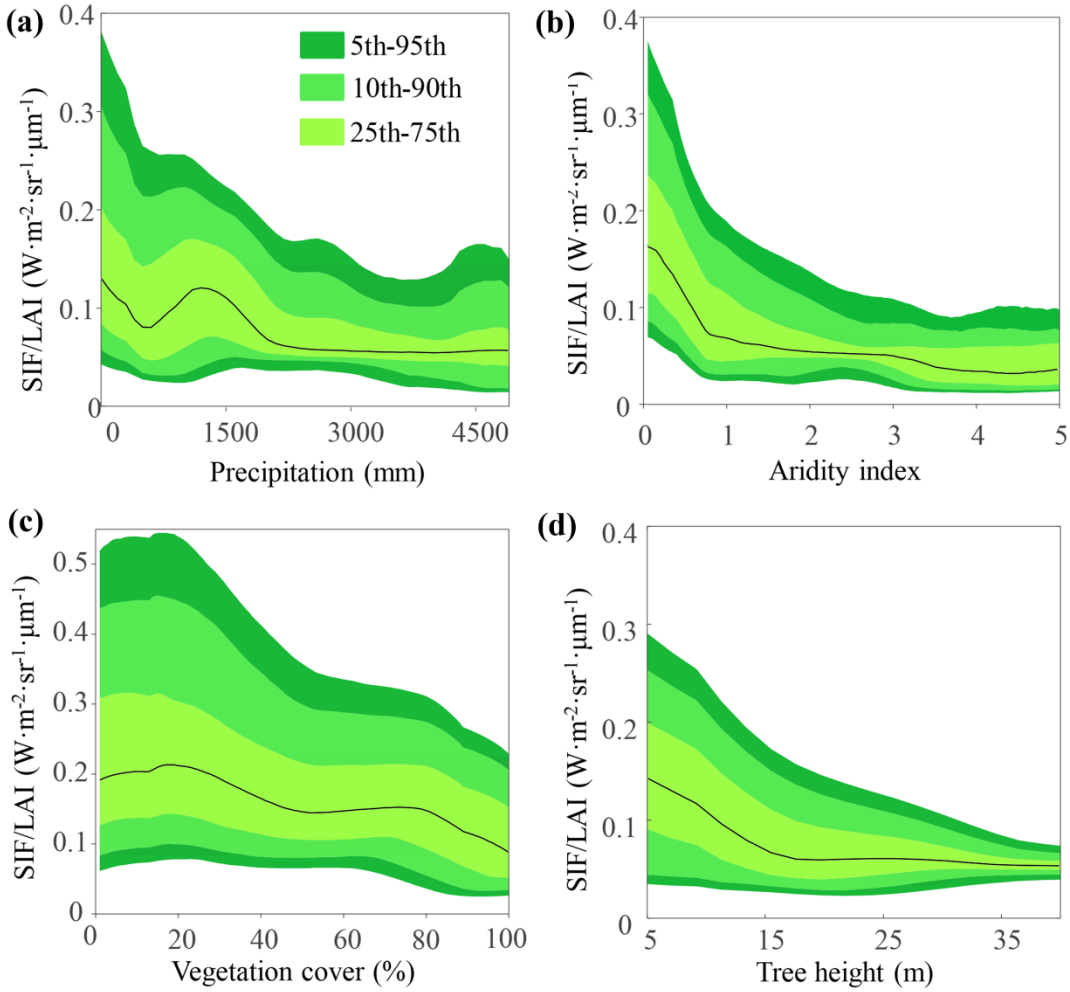


**Fig. S5.** Spatial relationships between ecosystem-scale photosynthetic efficiency (EPE) and potential drivers during 2001-2016. (a) precipitation, (b) aridity index, (c) vegetation cover, and (d) tree height. The black line is the median value.

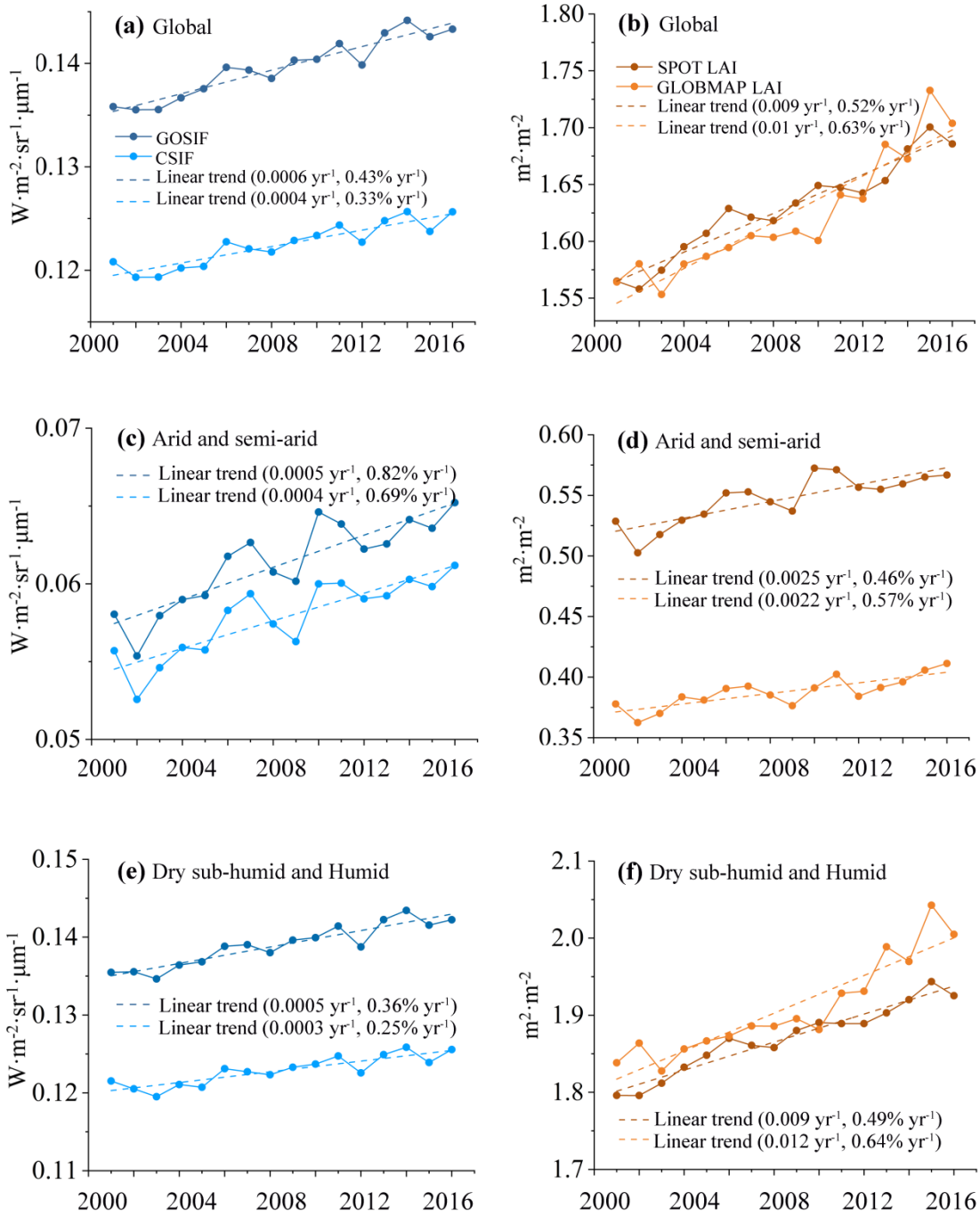


**Fig. S6.** Time series and linear trends of SIF and LAI during 2001-2016. SIF and LAI (a, b) at the global scale, (c, d) in arid and semi-arid areas, and (e, f) in dry sud-humid and humid regions.

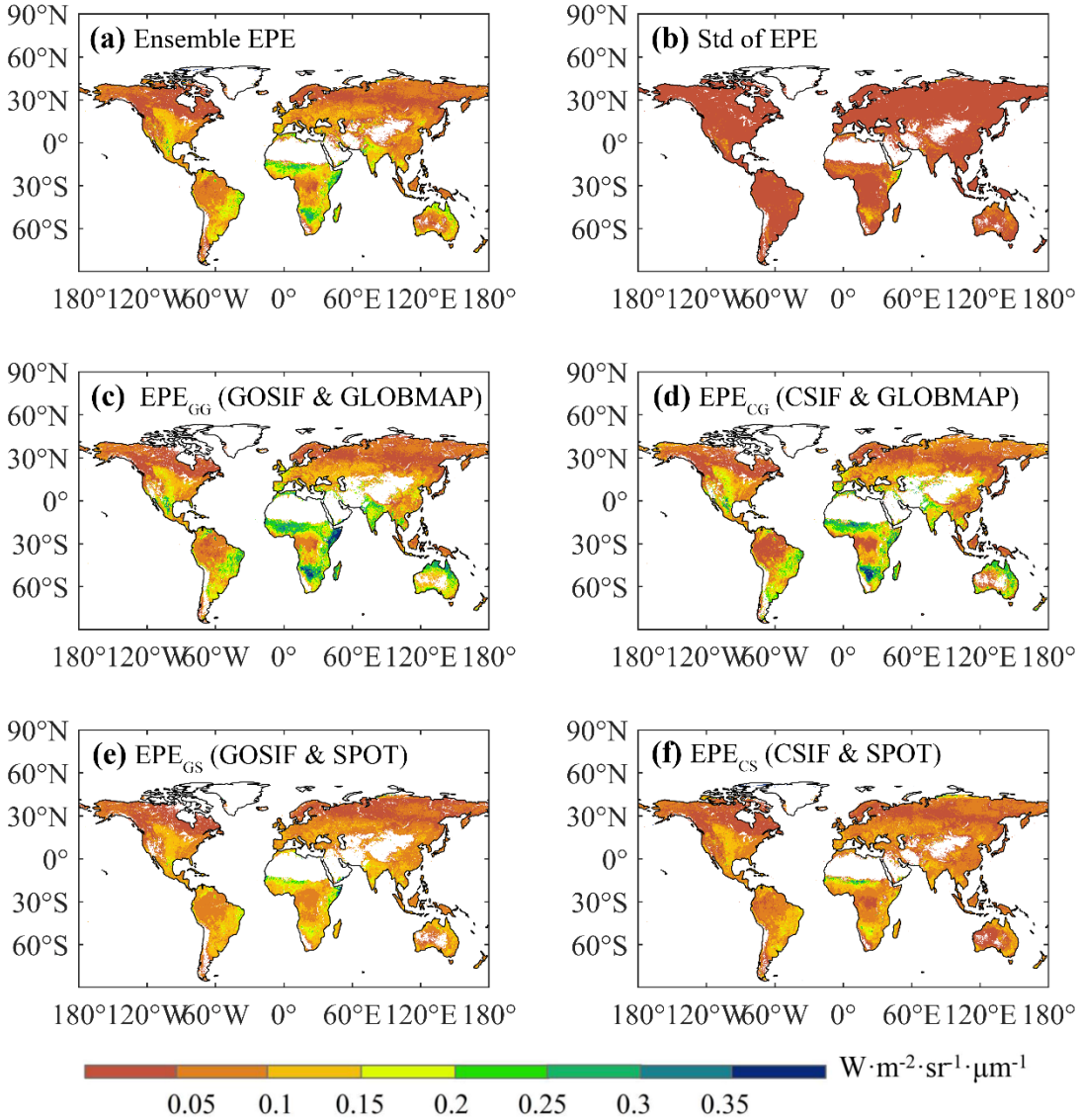


**Fig. S7.** Global pattern of ecosystem-scale photosynthetic efficiency (EPE) during 2001-2016. Maps of (a) the ensemble annual mean EPE, (b) the standard deviation of EPE, (c) $EPE_{GG}$ based on GOSIF and GLOBMAP LAI, (d) $EPE_{CG}$ based on CSIF and GLOBMAP LAI, (e) $EPE_{GS}$ based on GOSIF and SPOT LAI, and (f) $EPE_{CS}$ based on CSIF and SPOT LAI.

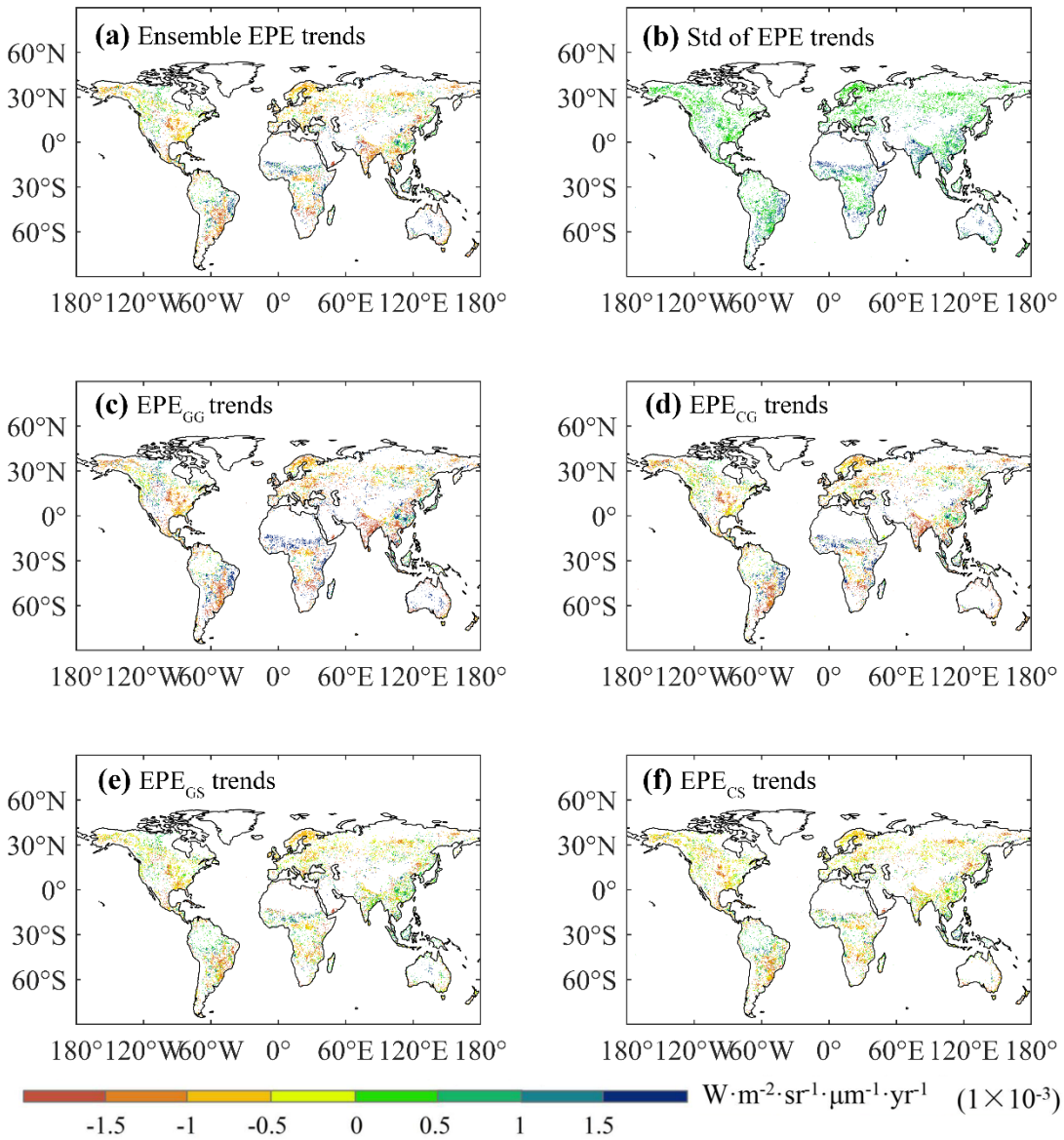


**Fig. S8.** Temporal dynamics of ecosystem-scale photosynthetic efficiency (EPE) during 2001-2016. Maps of (a) the ensemble EPE trends, (b) the standard deviation of EPE trends, (c) $EPE_{GG}$ trends based on GOSIF and GLOBMAP LAI, (d) $EPE_{CG}$ trends based on CSIF and GLOBMAP LAI, (e) $EPE_{GS}$ trends based on GOSIF and SPOT LAI, and (f) $EPE_{CS}$ trends based on CSIF and SPOT LAI.

**Table. S1.** Statistics of trends in ecosystem-scale photosynthetic efficiency (EPE) for different aridity classes. Percentage numbers in normal and boldface are relative (denominator is the area of each aridity class) and absolute (denominator is all pixels with the same trends) areal fraction.

| | Pixel numbers | Pixel numbers with significant changes in SIF/LAI | Pixel numbers with significant positive trends of SIF/LAI | Pixel numbers with significant negative trends of SIF/LAI | Percentage of significant trends in SIF/LAI | Relative percentage of significant positive trends of SIF/LAI | Percentage of significant positive trends of SIF/LAI | Relative percentage of significant negative trends of SIF/LAI | Percentage of significant negative trends of SIF/LAI |
|---|---|---|---|---|---|---|---|---|---|
| Arid | 788800 | 42322 | 32216 | 10106 | 5.37 | 76.12 | **9.37** | 23.88 | **1.55** |
| Semi-arid | 978100 | 157473 | 79706 | 77767 | 16.10 | 50.62 | **23.18** | 49.38 | **11.94** |
| Dry sub-humid | 636100 | 138550 | 47456 | 91094 | 21.78 | 34.25 | **13.80** | 65.75 | **13.99** |
| Humid | 3447600 | 650117 | 185349 | 464768 | 18.86 | 28.51 | **53.91** | 71.49 | **71.39** |

Table. S2 Statistics of trends in ecosystem-scale photosynthetic efficiency (EPE) for each land cover class. Percentage numbers in normal and boldface are relative (denominator is the area of each land cover type) and absolute (denominator is all pixels with the same trends) areal fraction.

| | pixel numbers | pixel numbers with significant changes in SIF/LAI | pixel numbers with significant positive trends of SIF/LAI | pixel numbers with significant negative trends of SIF/LAI | percentage of significant trends in SIF/LAI | Relative percentage of significant positive trends in SIF/LAI | percentage of significant positive trends of SIF/LAI | Relative percentage of significant negative trends of SIF/LAI | percentage of significant positive trends of SIF/LAI |
|---|---|---|---|---|---|---|---|---|---|
| ENF | 135258 | 35611 | 8385 | 27226 | 26.33 | 23.55 | **2.44** | 76.45 | **4.18** |
| EBF | 414065 | 78846 | 43008 | 35838 | 19.04 | 54.55 | **12.51** | 45.45 | **5.50** |
| DNF | 20208 | 5826 | 552 | 5274 | 28.83 | 9.47 | **0.16** | 90.53 | **0.81** |
| DBF | 115930 | 29979 | 7983 | 21996 | 25.86 | 26.63 | **2.32** | 73.37 | **3.38** |
| MF | 249984 | 65499 | 16781 | 48718 | 26.20 | 25.62 | **4.88** | 74.38 | **7.48** |
| TSH | 210879 | 21861 | 14886 | 6975 | 10.37 | 68.09 | **4.33** | 31.91 | **1.07** |
| ESH | 415548 | 28559 | 14838 | 13721 | 6.87 | 51.96 | **4.32** | 48.04 | **2.11** |
| TSA | 559492 | 192705 | 60879 | 131826 | 34.44 | 31.59 | **17.71** | 68.41 | **20.25** |
| ESA | 713792 | 180653 | 43770 | 136883 | 25.31 | 24.23 | **12.73** | 75.77 | **21.03** |
| TGR | 567722 | 126577 | 67646 | 58931 | 22.30 | 53.44 | **19.67** | 46.56 | **9.05** |
| EGR | 498940 | 63185 | 33980 | 29205 | 12.66 | 53.78 | **9.88** | 46.22 | **4.49** |
| CRO | 550255 | 165569 | 31 | 134455 | 30.09 | 18.79 | **9.05** | 81.21 | **20.65** |